ATP11c is critical for phosphatidylserine internalization and B lymphocyte differentiation

Mehmet Yabas, Charis E. Teh, Sandra Frankenreiter, Dennis Lal, Carla M. Roots, Belinda Whittle, Daniel T. Andrews, Yafei Zhang, Narci C. Teoh, Jonathan Sprent, Lina E. Tze, Edyta M. Kucharska, Jennifer Kofler, Geoffrey C. Farell, Stefan Bröer, Christopher C. Goodnow & Anselm Enders

Supplementary Figure 1

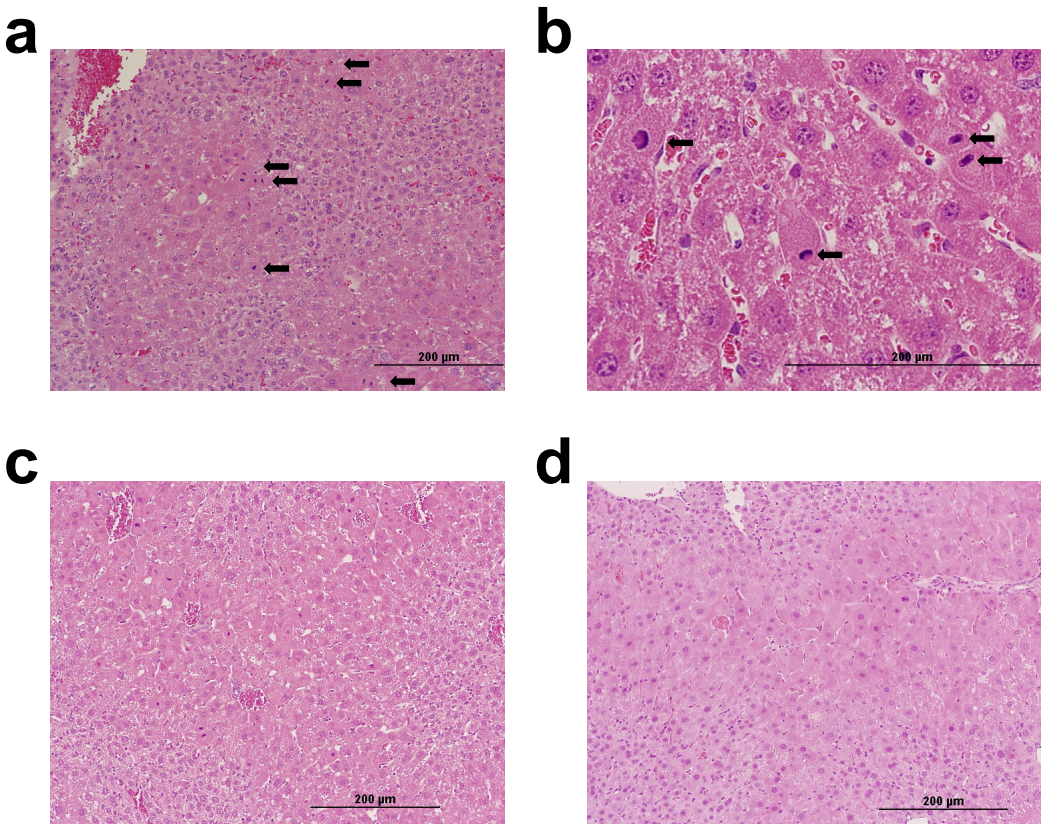

Supplementary Figure 1: (a) Multiple mitotic figures (indicated by arrowheads) seen in a representative H&E stained liver tumor section from a *Atp11c*$^{amb/0}$ mutant mouse (X200). **(b)** Abnormal mitotic figures with condensed, asymmetric chromatin at higher magnification (X400). **(c, d)** Representative H&E stained sections of *Atp11c*$^{amb/0}$ mutant hepatocellular carcinoma at 6 months (X200 magnification).

Supplementary Figure 2

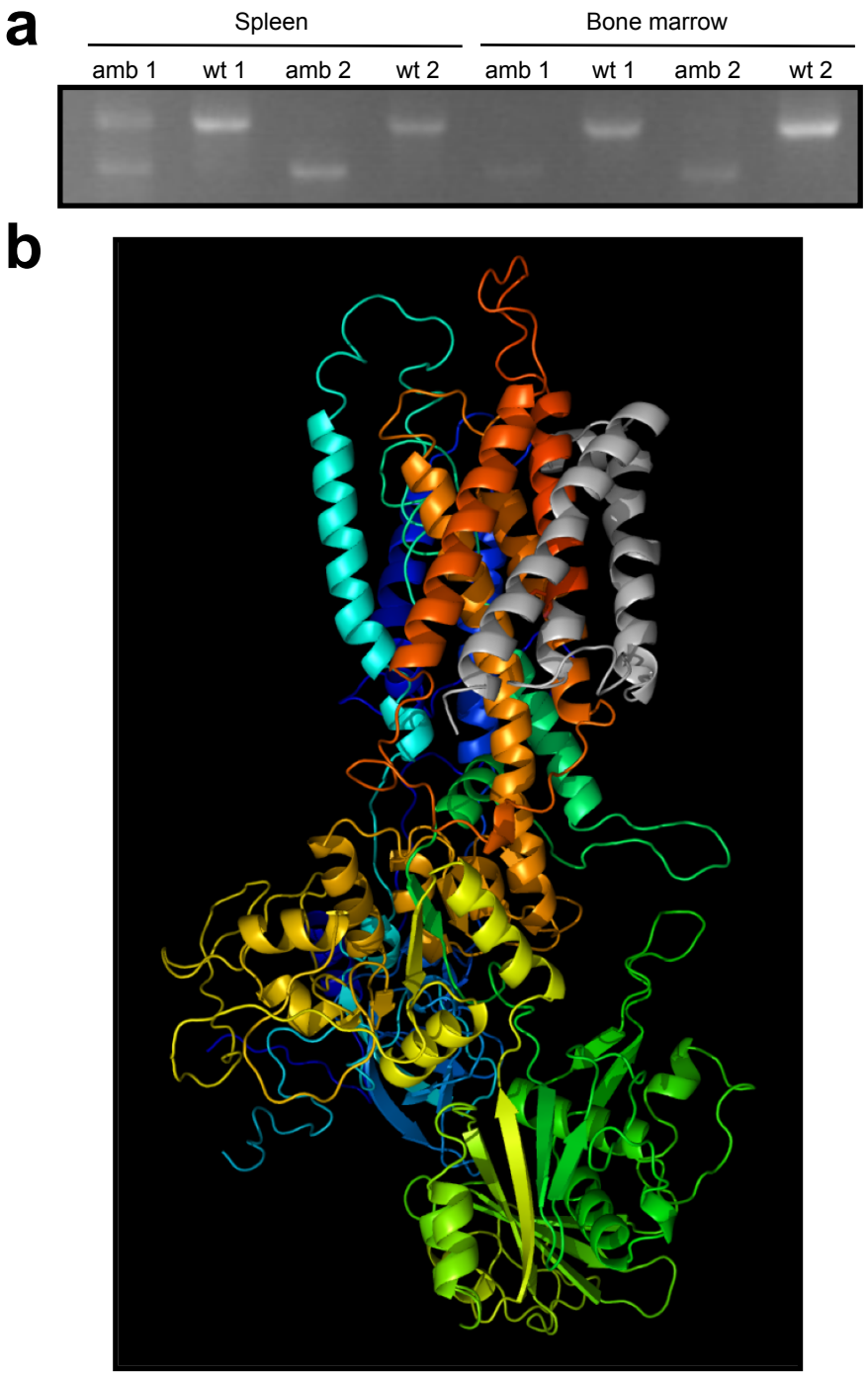

Supplementary Figure 2: Effect of the Atp11c^{amb} mutation on splicing and predicted consequence for ATP11c protein. (a) PCR products from spleen or bone marrow cDNA amplified with primers located in exons 25 and 29, showing shorter product in mutant animals (Amb) compared to wild-type (WT) animals. The cDNA was generated from RNA isolated from total splenocytes (left) or bone marrow (right). Some mutant animals had also a weak band at approximately the same size as the band observed in wild-type animals. Data is representative of two independent experiments with two animals per group and experiment. **(b)** Homology model of ATP11c based on the structure of the rabbit sacoplasmic-endoplasmic reticulum calcium ATPase 1 (ref. [45]). Residues marked in grey are predicted to be missing-altered from the mutant ATP11c proteins produced in both strains presented here.

Supplementary Figure 3

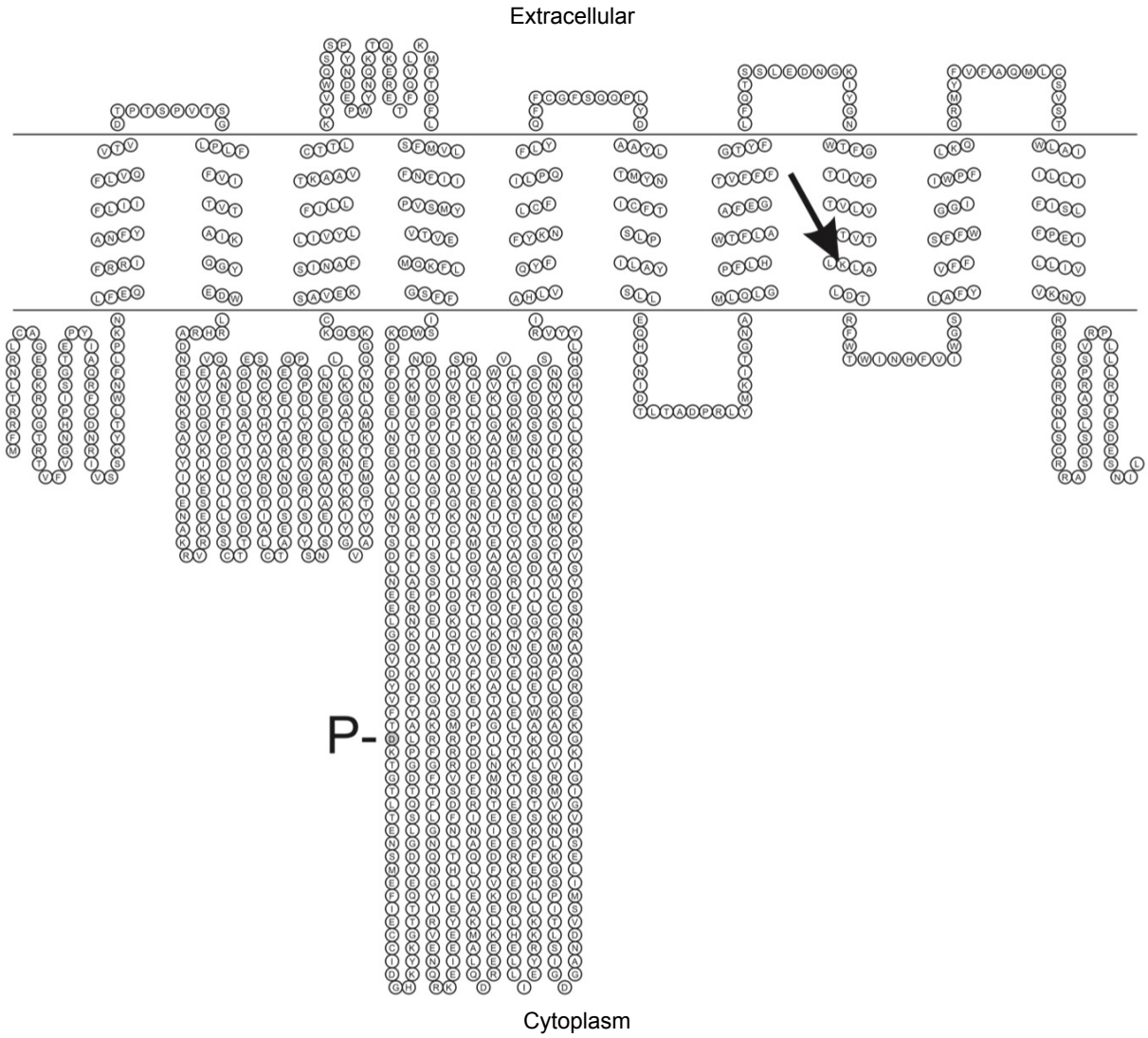

Supplementary Figure 3. Schematic of the predicted protein structure of ATP11c. The arrowhead point to the position of the predicted frameshift abolishing the C-terminal residues in the Atp11c^{amb} strain. The highlighted aspartic acid is phosphorylated during the catalytic cycle of the transport process.

Supplementary Figure 4

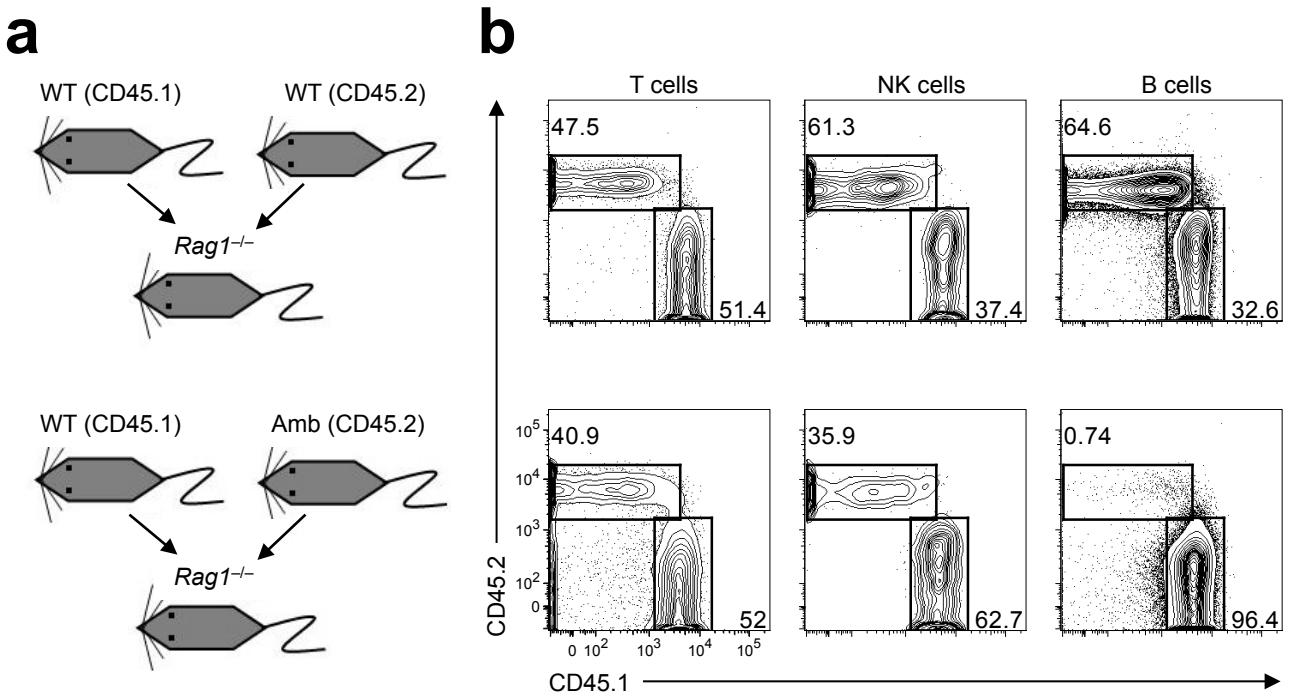

Supplementary Figure 4: B cell deficiency in *Atp11c*$^{amb/0}$ mice is due to a cell-autonomous requirement for ATP11c within B cells. (a) Bone marrow cells from CD45.1$^+$ wild-type (WT) mice was mixed with equal numbers of bone marrow cells from CD45.2$^+$ wild-type or *Atp11c*$^{amb/0}$ (Amb) mice and injected intravenously into irradiated *Rag1*$^{-/-}$ animals. **(b)** 12 weeks after reconstitution the mice were analyzed by flow cytometry for the percentage of CD45.1$^+$ versus CD45.2$^+$ CD3$^+$ T cells, NK1.1$^+$ NK cells and B220$^+$ B cells in the spleen. The data are representative of 2 independent experiments with 4 to 6 mice per group and experiment.

Supplementary Figure 5

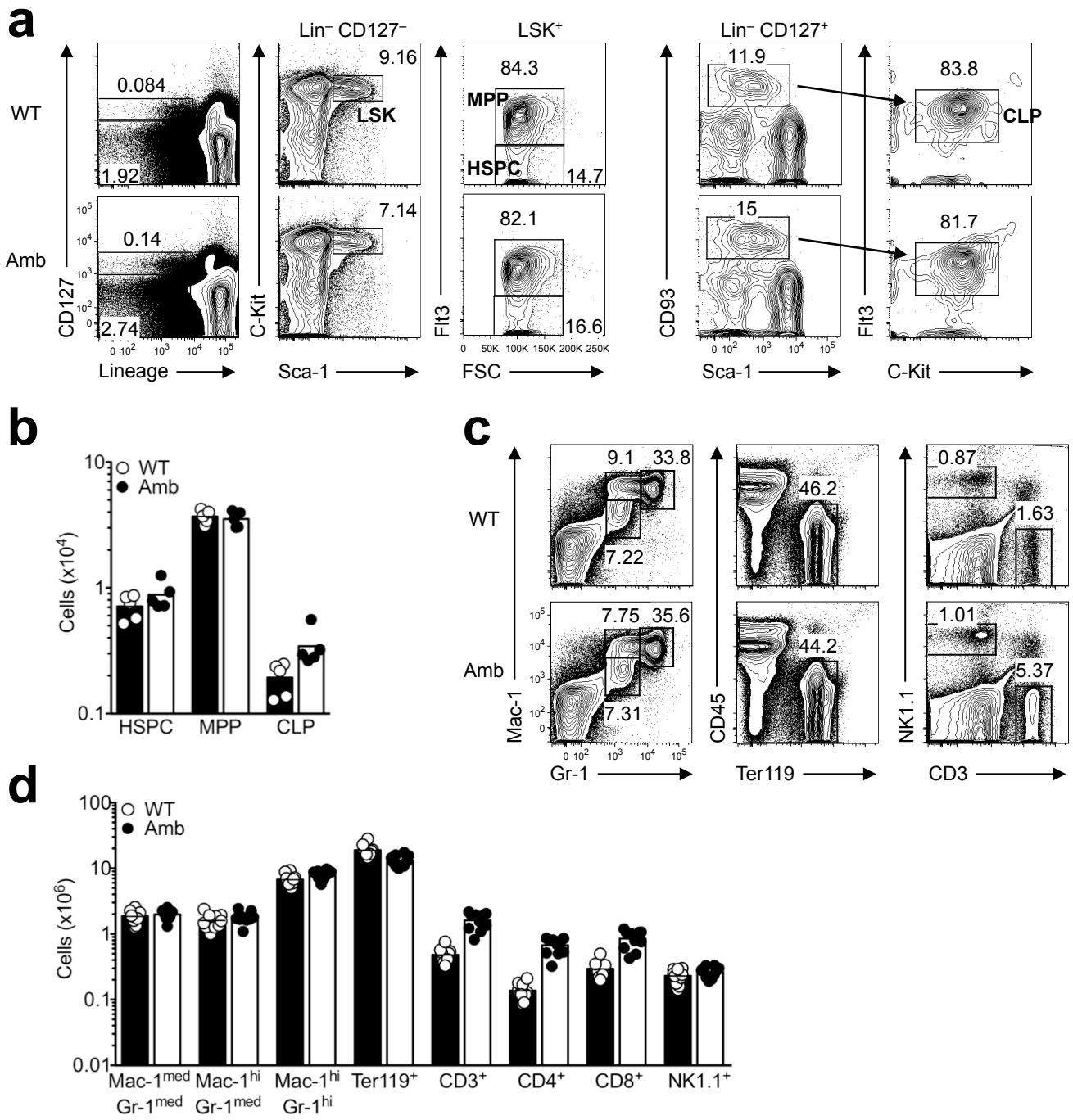

Supplementary Figure 5: Analysis of major blood cell progenitors and lineages in the bone marrow. (a) Representative flow cytometric analysis of the frequency of HSPC, MPP and CLP cells in the bone marrow of *Atp11c*$^{+/0}$ (WT) and *Atp11c*$^{amb/0}$ (Amb) mice. **(b)** Absolute number of the cell populations gated as in (a), from *n* = 5 mice of each genotype analyzed in two different experiments. Lineage panel for the analysis contains CD4, CD5, CD8, TCRb, TCRgd, IgM, IgD, B220, CD19, Mac-1, CD11c, Ter119, Ly6c, Gr-1 and NK1.1 **(c)** Representative flow cytometric analysis of the frequency of Myeloid cells (Mac-1^{med} Gr-1^{med}, Mac-1^{hi} Gr-1^{med} and Mac-1^{hi} Gr-1^{hi} respectively), Erythrocytes (Ter119^{+}), NK cells (NK1.1^{+}) and T cells (CD3^{+}) in the bone marrow of *Atp11c*$^{+/0}$ (WT) and *Atp11c*$^{amb/0}$ (Amb) mice. **(d)** The graph shows the absolute number of the indicated cell populations from *n* = 10 mice from each genotype analyzed in two different experiments.

Supplementary Figure 6

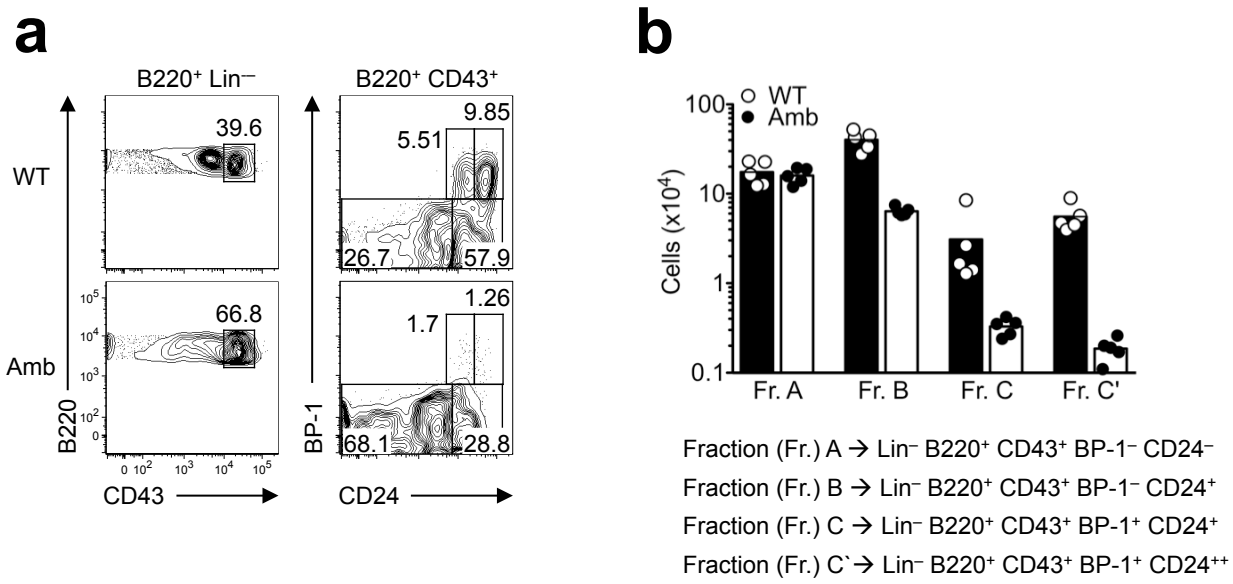

Fraction (Fr.) A → Lin⁻ B220⁺ CD43⁺ BP-1⁻ CD24⁻
Fraction (Fr.) B → Lin⁻ B220⁺ CD43⁺ BP-1⁻ CD24⁺
Fraction (Fr.) C → Lin⁻ B220⁺ CD43⁺ BP-1⁺ CD24⁺
Fraction (Fr.) C`→ Lin⁻ B220⁺ CD43⁺ BP-1⁺ CD24⁺⁺

Supplementary Figure 6: Analysis of B cell subpopulations in the bone marrow. (a) Representative flow cytometric analysis of B220, CD43, BP-1 and CD24 surface expression on bone marrow of mice from the indicated genotypes. Lineage panel for the analysis contains CD4, CD5, CD8, TCRb, TCRgd, IgM, Mac-1, CD11c, Ter119, Ly6c, Gr-1 and NK1.1 **(b)** The graph shows the absolute number of Fraction (Fr.) A-C′ cell populations shown in (**a**). The data are representative of 2 independent experiments with 2-5 mice per group and experiment.

Supplementary Figure 7

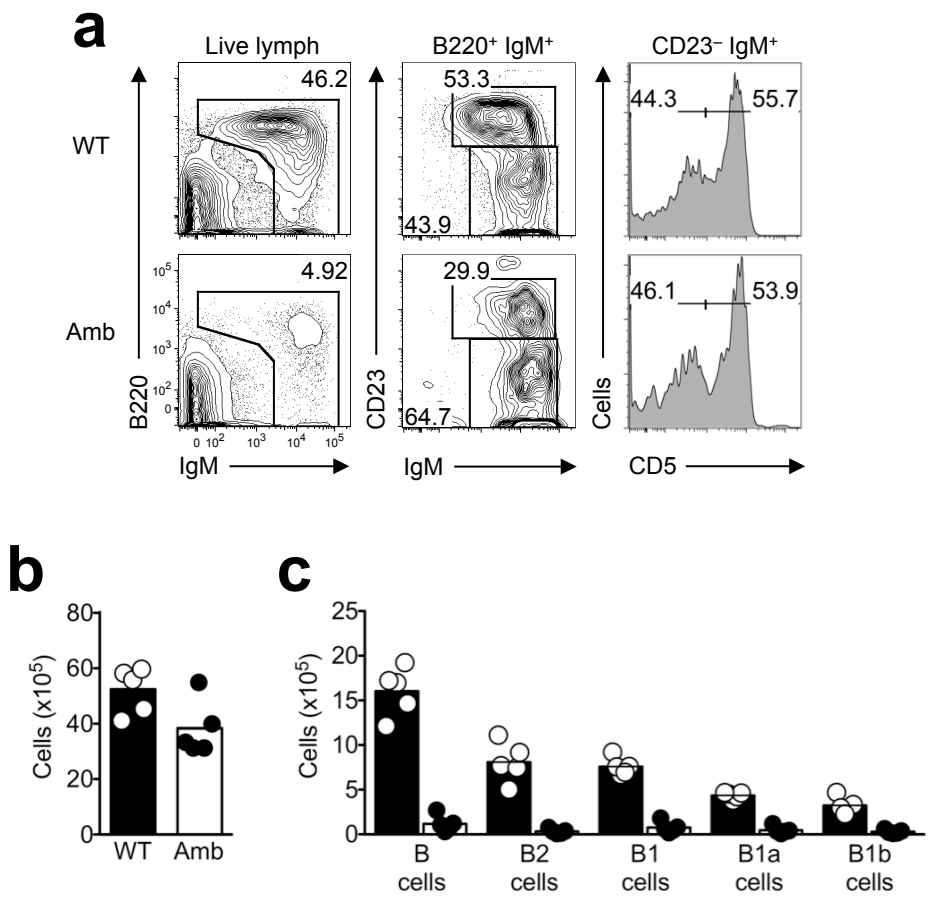

Supplementary Figure 7: Effect of the ATP11c^{amb} mutation on peritoneal B cells. (a) Representative flow cytometric analysis of the frequency of B cells and B cell subpopulation in the peritoneal cavity. Ambrosius mice have an approximately one-tenth of peritoneal B cells compared to wild-type mice and have an equal reduction of B1 (CD23^{-}) and B2 (CD23^{+}) B cells. The histogram shows the expression of CD5 on the B1 cells. **(b,c)** absolute cell numbers and number of B cells including subpopulations in the peritoneal cavity of wild-type (white circles) and ambrosius (black circles) mice. The data is representative of 2 independent experiments of 3-5 animals per group and experiment.

Supplementary Figure 8

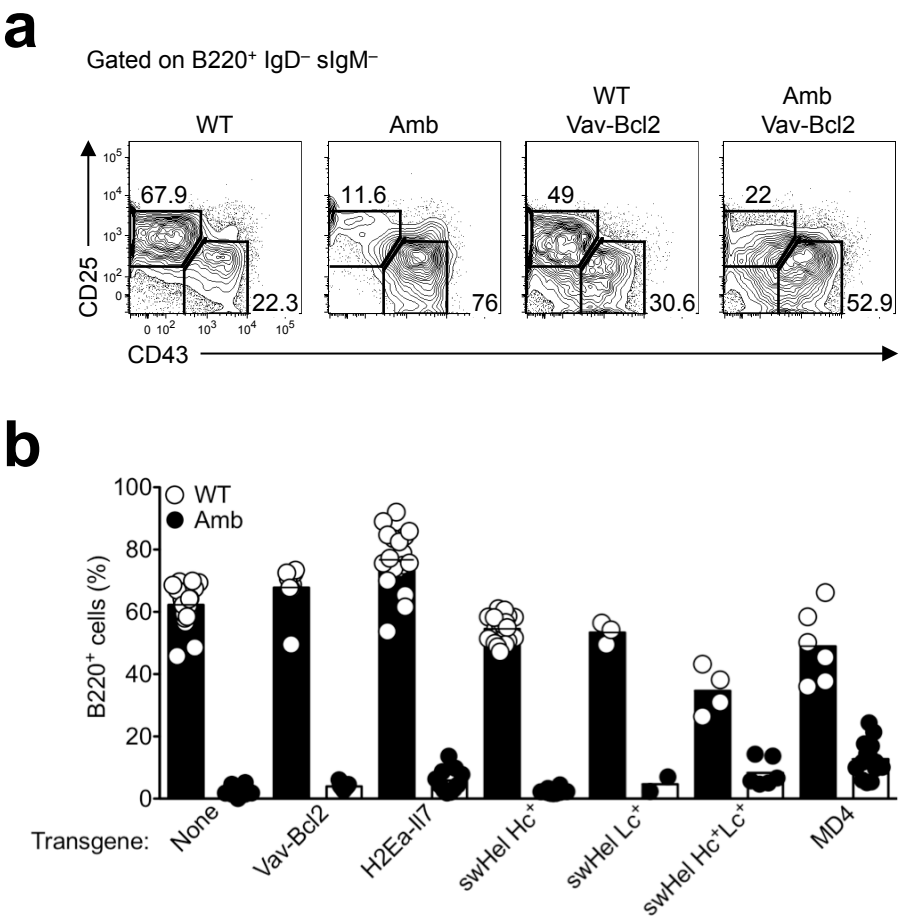

Supplementary Figure 8: Limited rescue of B cells in the blood by overexpression of either Bcl-2 or IL-7 or transgenic BCRs. (a) B220 $^{+}$ B cells (%) in the blood of mice from the indicated genotypes. *Vav-Bcl2* mice express Bcl-2 under the control of the *Vav* promoter, *H2Ea-Il7* mice express IL-7 under the control of the MHC class II Ea promotor. SW_{HEL} mice have a rearranged HEL-specific VDJ exon knocked into the heavy chain locus and a rearranged HEL-specific kappa light-chain transgene. The MD4 mice carry several copies of rearranged HEL-specific H and L chain transgenes, co-integrated a one site on Chromosome 17 several cM distal to *H2*. Each dote represents an individual animal. **(b)** Representative flow cytometric profiles of $sIgM^{–}$ $IgD^{–}$ $B220^{lo}$ bone marrow cells from mice of the indicated genotypes . The percentage of $CD25^{–}$ $CD43^{+}$ pro-B cells and $CD25^{+}$ $CD43^{-}$ pre-B cells is shown. Note that the *Vav-Bcl2* transgene increases the percentage of $CD43^{–}$ cells in Amb mutant animals, but these cells show little increase in CD25. The data are representative of 2 independent experiments with 2-3 mice per group and experiment.

Supplementary Figure 9

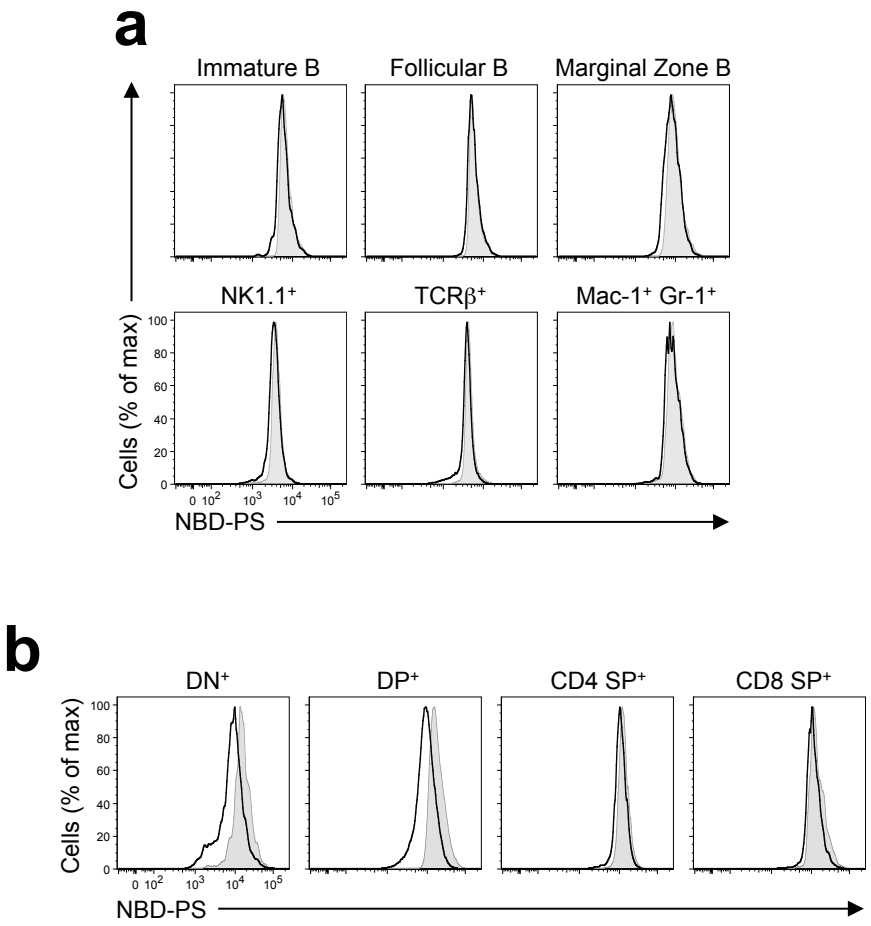

Supplementary Figure 9: ATP11c^{amb} mutation affects the rate of phosphatidylserine flipping in a lineage- and developmental stage-specific way. **(a)** Representative NBD-PS fluorescence profiles after 1 min incubation in immature B, follicular B, marginal zone B, NK, T and myeloid cells in the spleen from ATP11c mutant (black lines), compared to the corresponding CD45.1-marked wild-type cells in the same tube (shaded grey). **(b)** Representative NBD-PS fluorescence profiles after 1 min incubation in CD4 and CD8 double-negative (DN) or double-positive (DP), and CD4 or CD8 Single-positive (SP) cells, in the thymus from ATP11c mutant (black lines), compared to the corresponding CD45.1-marked wild-type cells in the same tube (shaded grey). The data are representative of 3 independent experiments.

Supplementary Figure 10

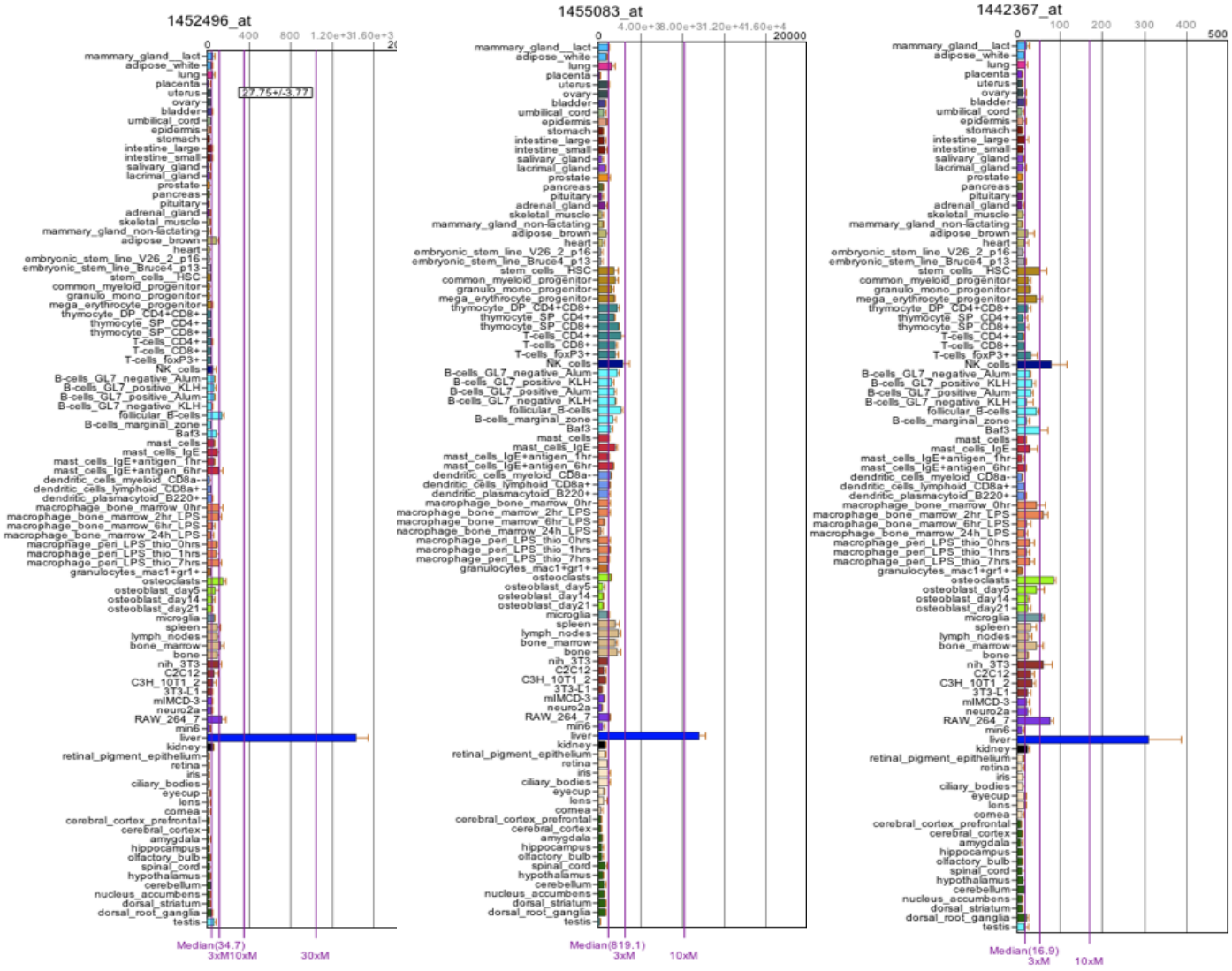

Supplementary Figure 10. BioGPS microarray data comparing Atp11c mRNA abundance in the indicated mouse tissues, using the indicated Affymetrix probesets. For details, see Wu C et al *Genome Biology* 2009, 10:R130.